Indian Journal of Biochemistry & Biophysics
Vol. 61, June 2024, pp. 354-370
DOI: 10.56042/ijbb.v61i6.8609

Some Co(II)-Schiff base complexes as promising anticancer agents: A DFT and molecular docking study

Pratyashee Barukial[1], Benzir Ahmed[1], Basanta Singha[2], Pankaj Chetia[3], Nipu Kumar Das[4], Samir Thakur[1], Upasana Bora Sinha[2] & Bipul Bezbaruah[1]*

[1]Department of Applied Sciences, Gauhati University, Guwahati-781 014, Assam, India

[2]Department of Chemistry, Nagaland University, Lumami-798 627, Nagaland, India

[3]Department of Life Sciences, Dibrugarh University, Dibrugarh -786 004, Assam, India

[4]Department of Chemical Engineering, Indian Institute of Technology, Guwahati-781 039, Assam, India

Received 07 February 2024; *revised 29 February 2024*

Non-covalent interactions have long been an emerging area of research in anticancer drug-DNA binding investigations since *in vivo* biomolecules are the primary target sites for all types of drug molecules. This study delves into the interaction of five promising Co(II)-Schiff base complexes (M_1-M_5) with DNA nucleobases, employing a multi-pronged approach to unveil their anticancer activity and interaction mechanisms. Density functional theory (DFT) provided a deep dive into the complexes' electronic structures, shedding light on how they interact with DNA nucleobases, their stability within these interactions, and the overall geometry involved. Further insights were gleaned from analysing frontier molecular orbitals (FMOs), molecular electrostatic potential (MEP), and non-covalent interactions (NCI) to investigate other important aspects of Co(II)-Schiff base complexes with the receptor AT/GC base pairs. Moreover, molecular docking simulations predicted the preferred binding sites and orientations of these complexes with B-DNA dodecamer, offering a realistic picture of their interactions with DNA in a larger context. Further, we also carried out Absorption, Distribution, Metabolism, Excretion, and Toxicity (ADMET) studies to analyse the pharmacokinetic and physicochemical properties of the Co(II)-Schiff base complexes. DFT study suggest that the Complex M_1 exhibits a strong affinity for both AT and GC base pairs, as indicated by its high negative interaction energy values of -18.55 kcal/mol for AT and -23.42 kcal/mol for GC.

Keywords: ADMET, AT/GC, DNA nucleobases, NCI, RDG

Metal complexes offer promising avenues for developing new anticancer agents. Researchers are constantly designing new "metallodrugs" with improved potency and reduced toxicity[1]. Metals like Ru, Pd, Rh, and Pt, *etc.*, when combined with the right donor ligands, can create versatile therapeutic agents with applications beyond pharmacology, such as in nanoscience, catalysis, molecular modelling, analysis of electronic and magnetic properties, *etc*[2,3]. These efforts are aided by the use of bioactive Schiff base derivatives, known for their excellent solubility as well as the capacity to form stable complexes with various metals, making them valuable tools in medicinal chemistry research[4]. Past literature reveals that Schiff base complexes with variable oxidation states of metal ions, *e.g.*, Zn^{+n}, Cu^{+n}, Ni^{+n}, Co^{+n}, Fe^{+n}, Mn^{+n}, and V^{+n} in their structural backbone, have a great impact on the interacting sites of any biologically active receptor[5]. Some reported metal complexes with Schiff base ligands *viz.*, N -(2-hydroxy-1- naphthylidene)-4-chloroaniline, N -(2-hydroxybenzylidene)-2,3- dimethylaniline, 2-hydroxy naphthaldehyde, PDH [N-(1-phenyl-2-hydroxy-2-phenylethylidine)-2′-hydroxy phenyl imine], HHP (N-(2-hydroxybenzylidine)-2′-hydroxy phenyl imine), N-(salicylidene)-2-hydroxyaniline, coumarin-thiazole, 2-methoxyethylamine derivatives, *etc.* show potential antibacterial, antituberculosis, anticancer and antitumour activity[5-9]. DNA's unique structure, specifically its nucleobases, makes it a prime target for new cancer therapies[10]. Metal complexes, particularly those containing cobalt, show potential in selectively interacting with DNA nucleobases, potentially disrupting the growth of cancer cells. Cobalt's unique properties, including its ability to change oxidation states (redox properties) and adapt its bonding (flexible valency), make it ideal for designing effective anticancer agents with minimal impact on healthy cells[11,12].

*Correspondence:
Phone: +91-9854634789 (Mob)
E-mail: bipulbezbaruah@gmail.com

An extensive array of experimental investigations has explored the multifaceted characteristics of Co(II)-Schiff base complexes as potential anticancer agents. Researchers such as El-Gammal *et al*. explored the anticancer efficacy of Ligand L_1, synthesized through the reaction between 2-hydrazino-2-oxo-N-phenylacetamide and 2-acetylpyridine in the presence of glacial acetic acid, leading to the formation of its tetrahedral Co(II) complex (M_1)[13]. Similarly, Revathi *et al*. synthesized a bidentate Schiff base, Ligand L_2, and utilized it to create a square planar cobalt(II) complex (M_2) via reaction with cobalt(II) acetate in methanol[14]. Abdel-Rahman *et al*. further contributed by synthesizing a nano-sized octahedral cobalt(II) complex (M_3) by combining Schiff base Ligand L_3 with cobalt nitrate[15]. Building upon this, Alks *et al*. characterized an octahedral cobalt(II) complex (M_4) by initially synthesizing Schiff base Ligand L_4 through condensation, and adding $CoCl_2 \cdot 6H_2O$[16]. Furthermore, Gaber *et al*. synthesized and characterized ligand L_5 through the reaction between chromone-3-carbaldehyde and 5-amino-1,3,4-thiadiazole-2-thiol, subsequently yielding an octahedral cobalt(II) complex (M_5) by introducing $CoCl_2 \cdot 6H_2O$ into an ethanol solution (Table 1A & B)[17]. Inspired by these investigations and the diverse properties reported for these complexes, we were motivated to delve deeper into the theoretical study of these Co(II)-Schiff base complexes.

This comprehensive study mainly focused on five Co(II)-Schiff base complexes (M_1-M_5) and their potential as anticancer agents. The chosen Schiff base ligands, including L_1 to L_5, exhibited diverse chemical structures and functionalities, as shown in (Table 1A & B)[13-17]. The potencies of the studied Co(II)-Schiff base complexes were evaluated using the standard IC_{50} method, which measures the concentration required for 50% inhibition (Table 2)[18,19]. Literature findings underscored the superior activity of these Co(II)-Schiff base complexes against cancer cell lines compared to their respective free ligands. Among them, the tetrahedral complex M_1 ($[Co(HL_1)Cl]$) displayed the highest toxicity towards EAC cells[13]. The square planar complex M_2 ($[Co(L_2)_2]$) demonstrated cytotoxicity against a broad spectrum of cancer cell lines, including HeLa (human cervical carcinoma), MCF-7 (human breast carcinoma), HEp2 (human laryngeal epithelial carcinoma) and, NHDF (normal human dermal fibroblast)[14]. The octahedral complexes M_3 ($[Co(L_3)(H_2O)_3]$), M_4 ($[Co(L_4)Cl(H_2O)_2]$), and M_5 ($[CoHL_5(Cl)_2(EtOH)_2]$) also exhibited promising anticancer properties against MCF-7, HCT-116 (human colon), Caco-2 (colon), and HepG2 (liver) cancer cell lines, respectively[15-17].

This study aims to investigate the interaction between some selected Co(II)-Schiff base anticancer agents and the nucleobase pairs, the building blocks

Table 1A — Chosen Schiff base ligands

Ligands	IUPAC name
L_1=HL_1	(Z)-2-oxo-2-(phenylamino)-N'-(1-(pyridin-2-yl) ethylidene acetohydrazide
L_2	2-(4,6-dimethylpyrimidin-2-ylimino)methyl)-4-nitrophenol
L_3	2-[(2-hydroxy-3-methoxy-benzylidene)-amino]-pyridin-3-ol
L_4	(4- (2-hydroxy-3-methoxy benzylidene)amino)pyrimidine-2-(1H)-on)
L_5=HL_5	3-{(5-mercapto-1,3,4-thiadiazol-2-ylimino) methyl}-4H-chromen-4-one

Table 1B − Studied Co(II)-Schiff base complexes

Co(II) Complexes	Molecular formula	Geometry
M_1	$[Co(HL_1)Cl]$	Tetrahedral
M_2	$[Co(L_2)_2]$	Square Planar
M_3	$[Co(L_3)(H_2O)_3)]$	Octahedral
M_4	$[Co(L_4)Cl(H_2O)_2]$	Octahedral
M_5	$[CoHL_5(Cl)_2(EtOH)_2]$	Octahedral

Table 2 — IC_{50} values of Co(II) Schiff base complexes

Co(II) complexes	IC_{50} or inhibition rate of the complexes on cancerous cells	IC_{50} or inhibition rate of the complexes on normal cells
M_1	164.52 μM in EAC cells	NA
	132.11 ± 10.34 μM in HEp2 cells	180.51 ± 9.74 μM in NHDF cells
M_2	139.34 ± 10.47 μM in HeLa	
	143.45 ± 14.99 μM in MCF-7	
M_3	9,280 μM in MCF-7	NA
	13,730 μM in MCF-7 cells	
M_4	609.6 μM in Caco-2 cells	1008.73 μM in L-929 cells
M_5	38.60 μM against HepG2 cells 9.26 μM in HepG2 cells	NA

of DNA. The primary objective of this study is to identify the preferred binding site of the specific nucleobase pairs with which the drug forms the strongest, most efficient interaction. By pinpointing the preferred binding site, one can gain valuable insights into drug's mechanism of action and potentially optimizing its effectiveness in targeting cancer cells. This information can be leveraged to model an anticancer agent and enhance its efficacy in selectively targeting cancer cells with limited harm to healthy tissues. DFT calculations provided insights into electron density distribution, while Reduced Electron Density Gradient (RDG) and Visual Molecular Dynamics (VMD) techniques helped visualize the preferred non-covalent interaction regions. In addition, molecular docking simulations shed light on potential hydrogen bonding and other weak intermolecular forces at play[20]. As an integral part of drug design processes, *in silico* ADME (absorption, distribution, metabolism, and excretion) pharmacokinetic properties, drug-likeness, medicinal compatibility, and toxicity profiling were also carried out for Co(II)-Schiff base complexes.

Materials and Methods

Density functional theory (DFT), has been used to analyse the interactions between molecules, to assess non-covalent interactions, including π-π stacking, between chosen Co(II)-Schiff base anticancer agents (M_1-M_5) and DNA nucleobases (AT and GC). The structures were initially constructed using GaussView5.0, and their optimization was initiated at the Becke 3-Lee-Yang-Parr (B3LYP) level of DFT with 6-31G basis set using Gaussian09 software[21,22]. Further, join Molecule and Arguslab software packages were used to generate and visualize all the stacked models[23]. The interaction energy for the stacked models of anticancer drugs and AT/GC base pair complexes can be calculated using the following equation:

$$\text{Interaction Energy, (IE)} = E_{AA\text{-}BP} - E_{AA} - E_{BP} \quad \ldots (1)$$

Where; $E_{AA\text{-}BP}$, E_{AA}, E_{BP} are the respective single point energies of the stacked anticancer agent-base pair complexes, anticancer agents, and AT/GC base pairs.

Additionally, the analysis included assessments of non-covalent interaction (NCI) and reduced density gradient (RDG) in order to examine repulsive and attractive interactions. The geographical distributions of electron density in systems with reduced electron density and gradient values are explained in depth using NCI analysis. The Multiwfn 3.8 software package was utilised to perform the studies[30]. The Visual Molecular Dynamics (VMD) programme was used to process the systems being analysed[31].

Results and Discussion

Analysis of interaction energies for stacked Co(II)-Schiff base Complexes with AT/GC base pairs

In this study, Co(II)-Schiff base complexes have been chosen with strong anticancer activity as they usually show non-covalent behaviour and π-π stacking interaction with AT/GC base pairs (Fig. 1); such molecular interaction is intended only through the intercalation mechanism within the DNA nucleobases. For any long-range interaction of DNA nucleobase, the favourable intermolecular separation typically ranges from 3.2-3.6Å; herein, it is kept at 3.6Å while constructing the Co(II) Schiff base-AT/GC stacked models. The computed interaction energy results for the stacked Co(II)-based Schiff base complexes, *viz.*, $[Co(HL_1)Cl]$, $[Co(L_2)_2]$, $[Co(L_3)(H_2O)_3)]$, $[Co(L_4)Cl(H_2O)_2]$ and $[CoHL_5(Cl)_2(EtOH)_2]$, with AT/GC base pairs are displayed in (Table 3). Energetically, in computational approaches, it is well known that for any stacked system; the more negative interaction energy value leads to the more stable stacked conformation. Hence, the sequence of stability of the stacked Co(II)-based Schiff base complexes with respect to the AT & GC base pairs is shown below:

For AT base pair: $M_5<M_3<M_4<M_2<M_1$

For GC base pair: $M_5<M_4<M_3<M_2<M_1$

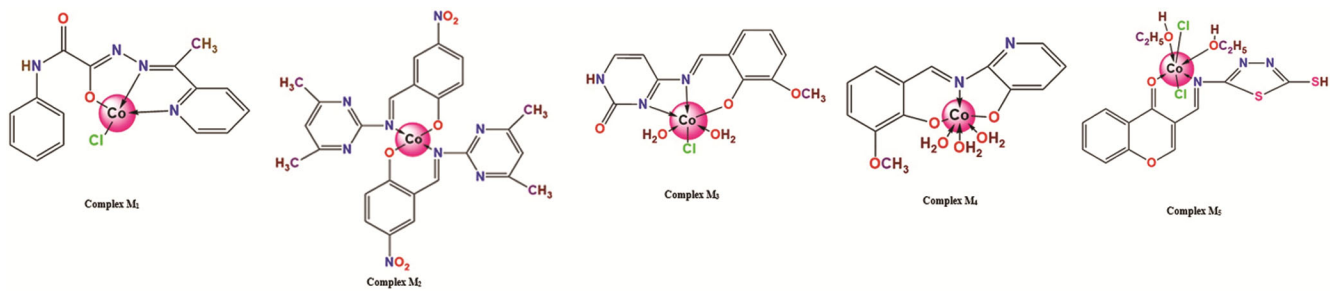

Fig. 1 — Optimized structures of the Co(II)-Schiff base anticancer agents

Table 3 — Computed Interaction energies (kcal/mol) for stacked Co(II)-Schiff base Complexes with AT and GC nucleobases

Co(II)- complexes	Interaction energy (kcal/mol)	
	AT	GC
M_1	-18.55	-23.42
M_2	-17.40	-21.43
M_3	-11.97	-16.14
M_4	-13.56	-15.79
M_5	-6.23	-9.57

From the above sequence of Co(II)-Schiff base-AT/GC stacked complexes, tetrahedral M_1 is found to be highly favoured and compatible to bind with both AT & GC base pairs, as it results in more negative interaction energy values of -18.55 and -23.42 kcal/mol, respectively, than that of other Co(II)-Schiff base anticancer agents. Again, for M_2, M_3 and M_4 complexes, the GC-stacked system results in the stacking interaction energy values of -21.43, -16.14 and -15.79 kcal/mol, which shows that these complexes give a less favourable stacked conformation as compared to M_1. Almost similar observations have also seen for AT-stacked systems, as the computed stacking interaction values are -17.40, -11.97 and -13.56 kcal/mol, *i.e.*, these complexes also result in less favoured stacked conformation than the M_1-GC stacked system. In contrast, the octahedral complex M_5 exhibits the most repulsive and least preferred stacked conformations, yielding less negative interaction energy values of -6.23 and -9.57 kcal/mol with respect to AT & GC base pairs since the octahedral geometry of M_5 is supposed to be overcrowded with bulky groups attached to the Co(II) ion. Hence, in complex M_5, the ligand intercalation mechanism takes place through the planar aromatic ring of the metal complex. Interestingly, the sequence of stability is greatly influenced by the molecular structure and geometry of the individual Schiff base ligands, too. For example, the stability of the most favoured M_1 complex with stacked AT/GC base pairs depends on the ligand L_1; as it intercalates within the DNA nucleobase through the N-based heterocyclic ring. But, for the least favoured Co(II)-Schiff base complex (M_5),intercalation takes place through the highly repulsive ligand L_5. The bar graph in Figure 2 clearly represents the variation in interaction energy values for the studied Co(II)-Schiff base complexes and AT/GC stacked systems.

HOMO-LUMO and Physicochemical analysis

Analysis of frontier molecular orbitals (FMOs) is widely acknowledged as a highly effective technique

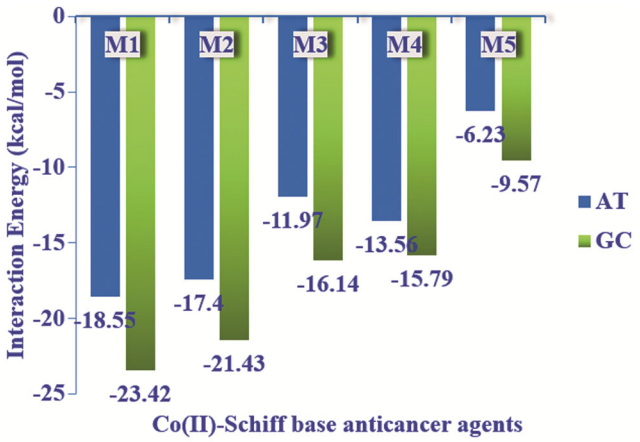

Fig. 2 — Interaction energy plots of Co(II)-Schiff base anticancer agents for AT/GC stacked systems

for identifying acceptor-donor interactions, as well as assessing molecular stability and reactivity. This approach has been implemented through exploration of the highest occupied molecular orbital (HOMO) and lowest unoccupied molecular orbital (LUMO). A species nucleophilic or electron-donating inclination is reflected by its highest occupied molecular orbital (HOMO), whereas its electrophilic or electron-accepting inclination is characterised by its lowest unoccupied molecular orbital (LUMO). A larger HOMO-LUMO energy gap results in higher molecular kinetic stability, lower chemical reactivity, and improved resistance to charge transfer. The HOMO-LUMO energy gap (E_{Gap}) determines different chemical reactivity descriptors of the metal complexes, such as chemical potential (μ), chemical hardness (η), chemical softness (S) and electrophilicity index (ω); that can be calculated by using the following equations[24]:

$$\text{Chemical Potential, } (\mu) = \frac{1}{2}(E_{LUMO} + E_{HOMO}) \quad \ldots (2)$$

$$\text{Chemical Hardness, } (\eta) = \frac{1}{2}(E_{LUMO} - E_{HOMO}) \quad \ldots (3)$$

$$\text{Chemical Softness (S)} = \frac{1}{\eta} \quad \ldots (4)$$

$$\text{Electrophilicity index } (\omega) = \frac{\mu^2}{2\eta} \quad \ldots (5)$$

Literature reveals that the E_{Gap} can be used to identify the chemical hardness and softness; a larger E_{Gap} represents a hard molecular complex, whereas soft molecules have a tiny energy gap[25]. Also, the chemical potential (μ) is the energy of a system owing to an electron change; if the μ value of a molecule is high, then it behaves as a strong electron donor, whereas, a low μ value represents a strong electron acceptor entity. Moreover, the quality of Softness (S)

is also important in determining the toxicity of any contaminants present in a molecular system[26].

The computed E_{Gap} and some of the chemical reactivity parameters for the stacked and unstacked Co(II)-Schiff base complexes are shown in (Table 4A-C). It has revealed that amongst all the selected Co(II)-metal complexes; M_1 has a low E_{Gap} (0.4435 eV), indicating that it is a soft molecule, whereas, M_2 is hard with a large energy gap (0.9121 eV) as shown in (Fig. 3 and Table 4A). Hence, we consider that M_2 shows better kinetic stability and is chemically less reactive as compared to other complexes. The chemical potential (μ) value of a molecule is directly related to the electron donor-acceptor behaviour of the molecular entity. Herein, M_2 has a strong electron acceptor system, while M_3 is a strong electron donor with μ values of -13.6757 and -6.9673 eV, respectively. A higher chemical hardness (η) value indicates greater stability, whereas, a lower chemical hardness (η) value refers greater reactivity;

Table 4A − Energies E_{HOMO}, E_{LUMO} and E_{Gap} for the studied unstacked Co(II)-Schiff base complexes

Co(II)-Schiff base complexes	E_{LUMO} (eV)	E_{HOMO} (eV)	E_{Gap} (eV)
M_1	-11.5286	-11.9721	0.4435
M_2	-13.2197	-14.1318	0.9121
M_3	-6.6028	-7.3317	0.7290
M_4	-12.7237	-13.3024	0.5788
M_5	-13.0173	-13.9038	0.8865

Table 4B − Chemical reactivity indices (μ), (η), (s) and (ω) for the studied individual Co(II)-Schiff base complexes

Co(II)-Schiff base complexes	Chemical Potential (μ)	Chemical Hardness (η)	Softness (s)	Electrophilicity index (ω)
M_1	-11.7504	0.2218	4.5093	311.3054
M_2	-13.6757	0.4560	2.1928	205.0546
M_3	-6.9673	0.3645	2.7437	66.5920
M_4	-13.0130	0.2894	3.4557	292.5917
M_5	-13.4605	0.4433	2.2561	204.3825

Table 4C − Chemical reactivity indices (μ), (η), (s)and (ω) for the minimized stacked Co(II)-Schiff base-AT/GC base pair complexes

Minimized stacked Co(II)-Schiff base-AT/GC complexes	Chemical Potential (μ)	Chemical Hardness (η)	Softness (s)	Electrophilicity (ω)
M_1-AT	-11.5157	0.3043	3.2858	217.8636
M_1-GC	-11.5591	0.3341	2.9928	199.9354
M_2-AT	-11.4591	0.2360	4.2364	278.1453
M_2-GC	-11.4630	0.2367	4.2243	277.5371
M_3-AT	-5.7669	0.0672	14.8790	247.4158
M_3-GC	-5.7658	0.0664	15.0620	250.3633
M_4-AT	-10.7017	0.3325	3.0075	172.2167
M_4-GC	-10.6992	0.3322	3.0099	172.2789
M_5-AT	-10.9783	0.1163	8.5968	518.0530
M_5-GC	-10.9157	0.0559	17.8838	1065.4493

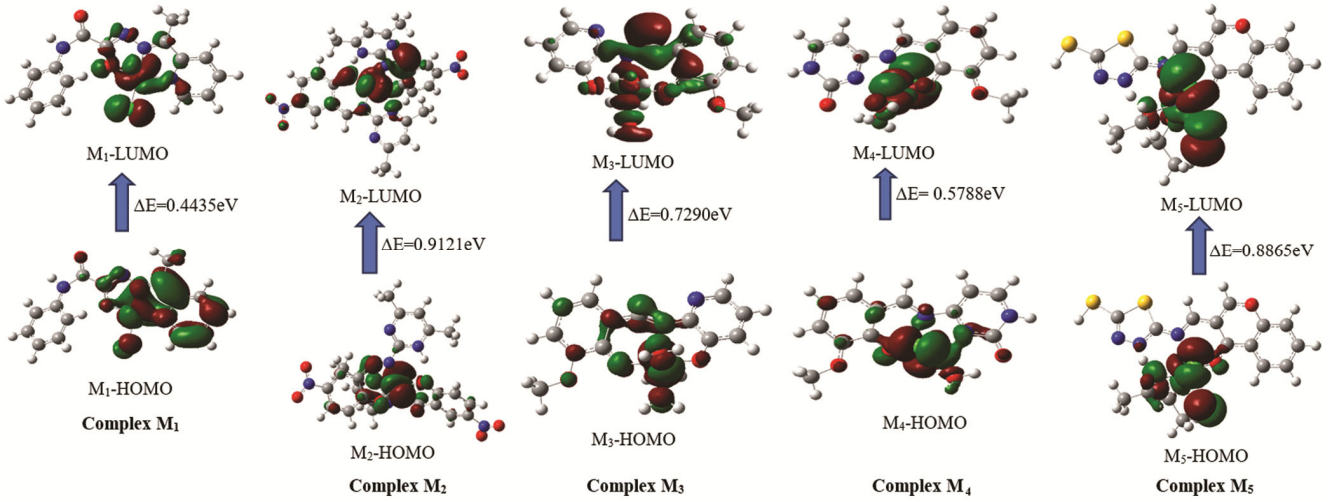

Fig. 3 — HOMO-LUMO diagrams of Co(II)-Schiff base complexes

hence, M_2 is considered as chemically harder or stable (η= 0.4560 eV) as compared to the other complexes. Again, the chemical softness (S) is the reciprocal of chemical hardness (η), which represents the degree of chemical reactivity of a molecular system; M_1 is chemically soft or reactive with a higher S value of 4.5093 eV^{-1} as compared to the other complexes. Further, for the most favoured M_1-GC stacked complex in (Table 4C), the computed chemical hardness (η) value is found to be 0.3341 eV; which is significantly higher than that of the unstacked M_1 with η value of 0.2218eV in (Table 4B). Moreover, the η value for M_1 with AT/GC stacked complex ranges from 0.3043 to 0.3341eV, which indicates the better stability of M_1 stacked systems than that of other anticancer agents as shown in (Table 4B-C). Contrary to that, M_1-AT/GC stacked system exhibits lower chemical softness (S) value ranges from 2.9928 to 3.2858 eV^{-1}, than that of unstacked M_1 complex, *i.e.*, 4.5093 eV^{-1}. Hence, M_1 is found to be softer than its M_1-AT/GC stacked molecular complexes. Again, the computed chemical potential (μ) values for the M_1-AT & M_1-GC stacked complex is found to be -11.5157 and -11.5591 eV, respectively**,** which reveals its strong electron accepting behaviour; but, interestingly unstacked M_1 also shows electron accepting nature with a negative μ value of -11.7504 eV. Again, M_1-AT & GC stacked system has a higher electrophilicity index (ω) ranging from 217.8636 to 199.9354 eV, which refers its electrophilic nature. Therefore, the computed μ and ω values confirms the chemical stability and electrophilic nature of its stacked system (Table 4C).

Natural Bond Orbital (NBO) analysis

The NBO approach can determine the level of hyper-conjugative interactions between an occupied molecular orbital and adjacent unoccupied orbital to analyse the intra or intermolecular interactions[27]. The stabilization energy (*E* (2)) for each donor (i) and acceptor (j) associated with the delocalization, i and j are estimated as shown below,

$$E^{(2)}= \Delta E_{ij} = q_i \frac{F(i,j)^2}{\varepsilon_j - \varepsilon_i} \quad \text{... (6)}$$

Where, q_i= donor orbital occupancy, $F(i,j)$= off-diagonal NBO Fock matrix element, $\varepsilon_j, \varepsilon_i$= diagonal elements.

The NBO analysis has been performed at the B3LYP/6-31G level in order to calculate the electronic charge distribution and intermolecular interaction of a donor-acceptor complex, as well as the extent of internal charge transfer (ICT) within an anticancer agent-AT/GC base pair stacked system. The NBO analysis of the most favoured M_1-AT&GC stacked complexes show πC_{37}-N_{38} →LP*(1)H_{59}(AT) and LP(2)O_{48} → σ*H_{49}-N_{52}(GC) electronic transition with stabilization energies of 28.70 and 17.33 kcal/mol, respectively, as shown in (Table 5). But, for the unstacked M_1 complex the most favoured electronic charge transition occurs through LP(1) C_{26} → π*C_{25}-C_{27} transition, *i.e.* 74.43 kcal/mol. Hence, we observe the relative changes occur in perturbation energy values that provide insight into electron donor-acceptor behaviour and charge transfer processes within the most favoured M_1-AT/GC stacked complex.

Molecular Electrostatic Potential (MEP) analysis

Molecular electrostatic potential (MEP) is a well-known indicator for the visual comprehension of physicochemical features *viz.*, molecular size, shape, electron density, relative polarity, electrophilic-nucleophilic sites, electrostatic potential regions and molecular interactions[28]. An electron-rich (negative) region, being the preferred site for an electrophilic attack is represented by the coloured; whereas electron deficient (positive) blue-coloured region refers a nucleophilic attack and electrostatically neutral region is represented by green colour as displayed in (Fig. 4). Usually, MEP can be analysed by observing the colour changes of a molecule; In Figure 4, the colour code of

Table 5 − NBO analysis for the unstacked and stacked M_1 complex

	Donor NBO (i)	Acceptor NBO (j)	E(2) Kcal/mol	E(j)-E(i) a.u.	F(ij) a.u.
Unstacked M_1	LP(1)C_{26}	π*C_{25}-C_{27}	74.43	0.08	0.116
	LP(1)N_{18}	LP*(6)Co_{19}	55.85	0.67	0.253
	πC_{43}-N_{46}	π*N_{44}-C_{45}	18.50	0.29	0.095
M_1-AT stacked	πC_{37}-N_{38}	LP*(1)H_{59}	28.70	0.39	0.147
	σC_{37}-H_{60}	LP*(1)H_{59}	27.37	0.64	0.204
	LP*(1)H_{59}	σ*C_{37}-H_{60}	7.34	0.32	0.097
M_1-GC stacked	LP(2)O_{48}	σ*H_{49}-N_{52}	17.33	0.71	0.143
	LP(1)O_{48}	σ*H_{49}-N_{52}	7.02	1.06	0.110
	σ*N_{46}-H_{64}	σ*H_{49}-N_{52}	2.54	0.03	0.033

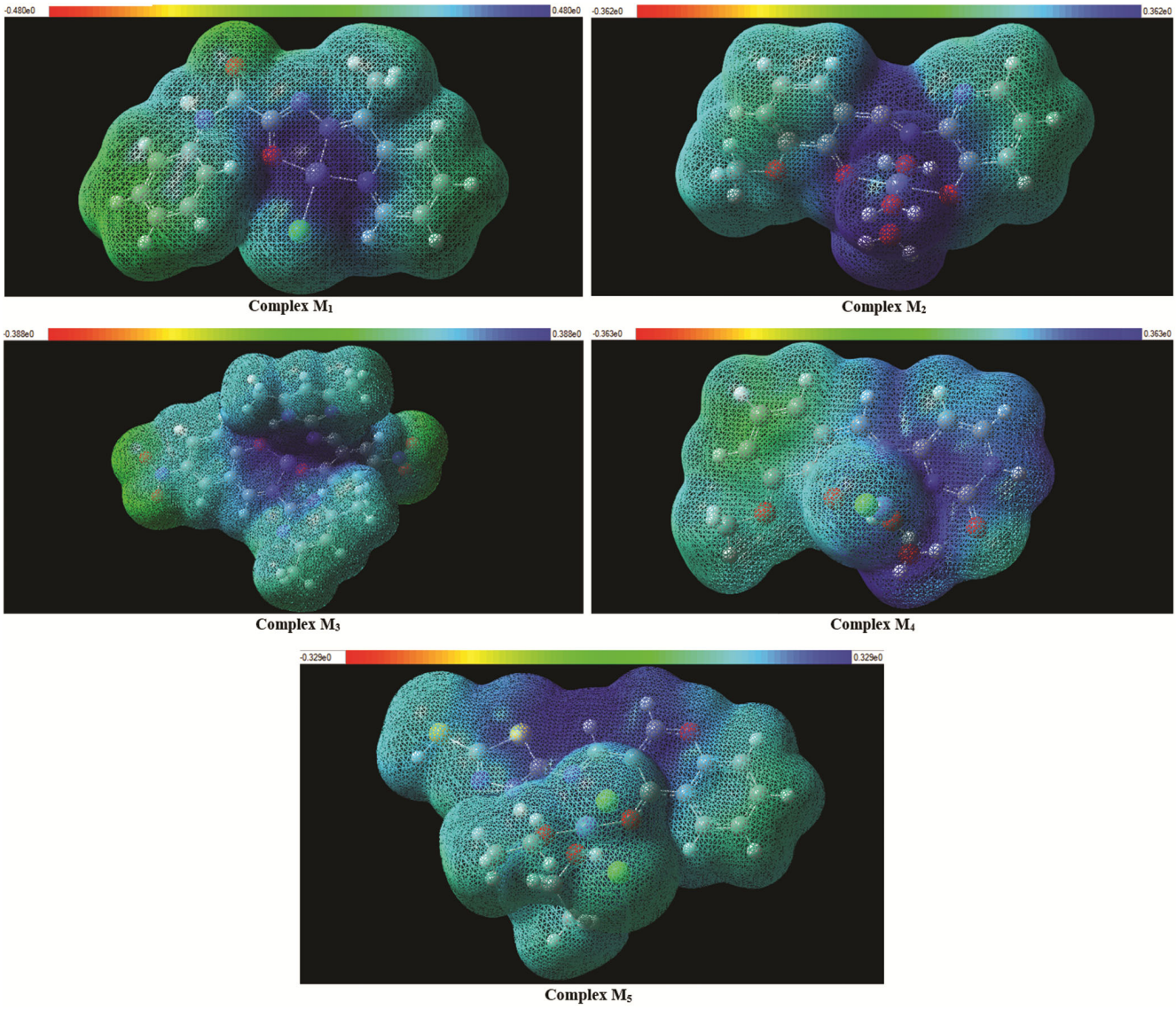

Fig. 4 — Molecular electrostatic potential (MEP) maps of Co(II)-Schiff base anticancer agents

the map is in the range between-0.480e0 (deepest red) and 0.480e0 a.u (deepest blue) for M_1 complex. Similarly, -0.362e0 (deepest red) and 0.362e0 a.u (deepest blue) for M_2, -0.388e0 (deepest red) and 0.388e0 a.u (deepest blue) for M_3, -0.363e0 (deepest red) and 0.363e0 a.u (deepest blue) for M_4, -0.329e0 (deepest red) and 0.329e0 a.u (deepest blue) for M_5 complexes. Hence, from the computed MEP diagrams, it was observed that all of the metal complexes have an active electropositive region which is the probable interacting sites for AT/GC base pairs (Fig. 4).

Non-covalent interaction (NCI) and Virtual molecular dynamics (VMD) analysis

Non-covalent interaction (NCI) and reduced density gradient (RDG) analysis provide vital insight into the molecular interactions which can be used to characterise weak intermolecular interactions. The molecular bonding and non-bonding interaction regions are evaluated by the reduced density gradient (S), which is represented by using NCI approach as described by the following equation[29]:

$$S = \frac{1}{2(3\pi^2)^{\frac{1}{3}}}\left(\frac{|\nabla^2\rho(r)|}{\rho(r)^{\frac{4}{3}}}\right) \quad \ldots (7)$$

Again, the Multiwfn and VMD programs were used to display the relevant coloured RDG scatter diagrams and 3D isosurfaces; where blue and red colour represents attractive and repulsive forces, respectively[30,31]. We can explore more about the nature and potency of molecular interactions by quantifying the electron density of the sign $\lambda_2\rho$ peaks

concerning RDG; where $\lambda_2\rho > 0$ denotes a repulsive non-bonded interaction and $\lambda_2\rho < 0$ refers repulsive bonding interaction[32]. The isosurface ranges between -0.035-0.020 a.u and the NCI studies were conducted at an isosurface value of 0.5 a.u. For each Co(II) Schiff base-AT/GC stacked complexes, there observed strong intermolecular interactions, where RDG points were plotted against electron density multiplied by the sign of second eigen value (sign(λ_2)ρ) and NCI plot as shown in (Fig. 5). The NCI plots of Co(II) Schiff base-AT/GC stacked complexes were represented by the isosurfaces using

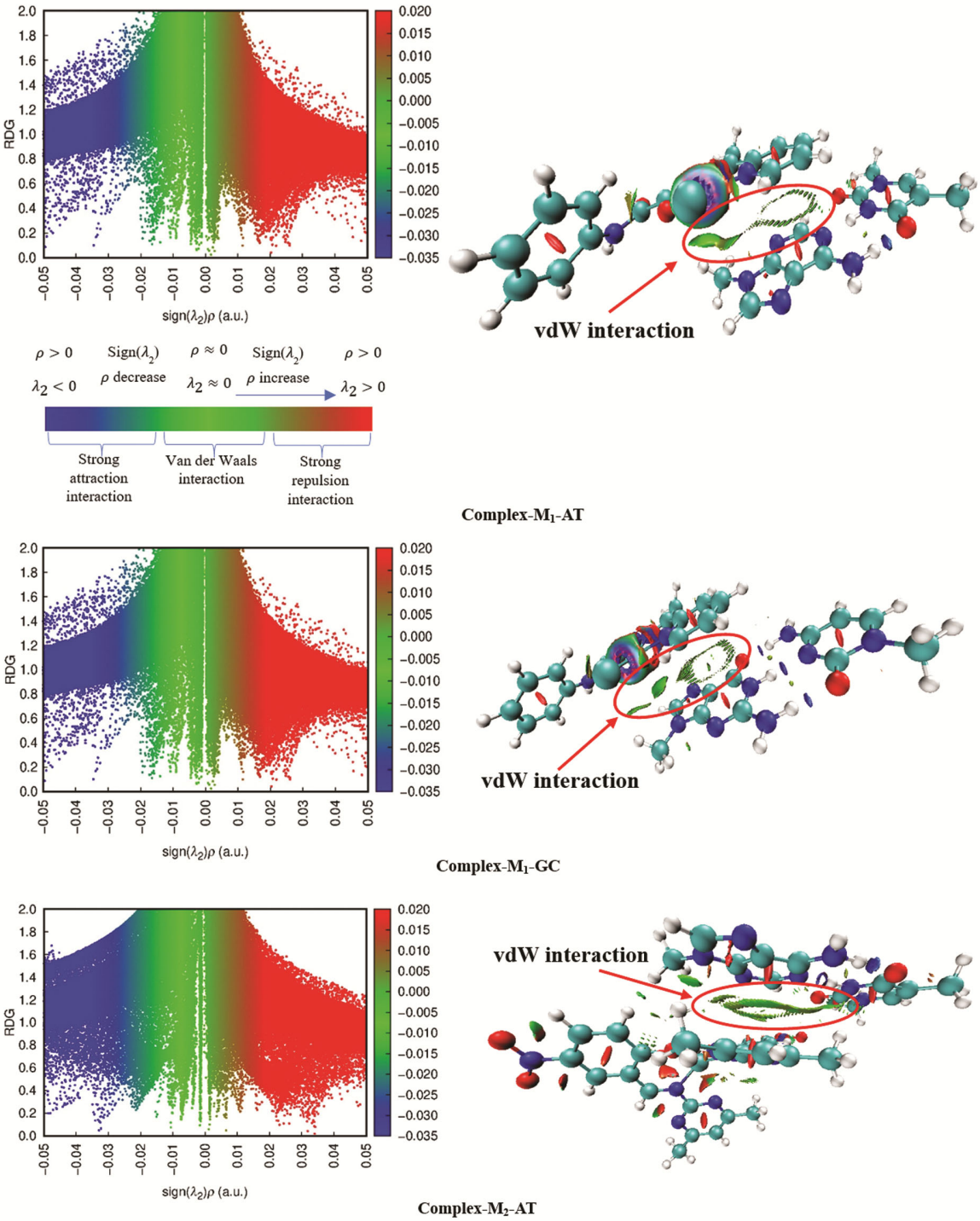

Fig. 5 — RDG scatter plots (left) and VMD plots (right) of stacked Co(II)-Schiff base-AT/GC base pair complexes (*Contd*.)

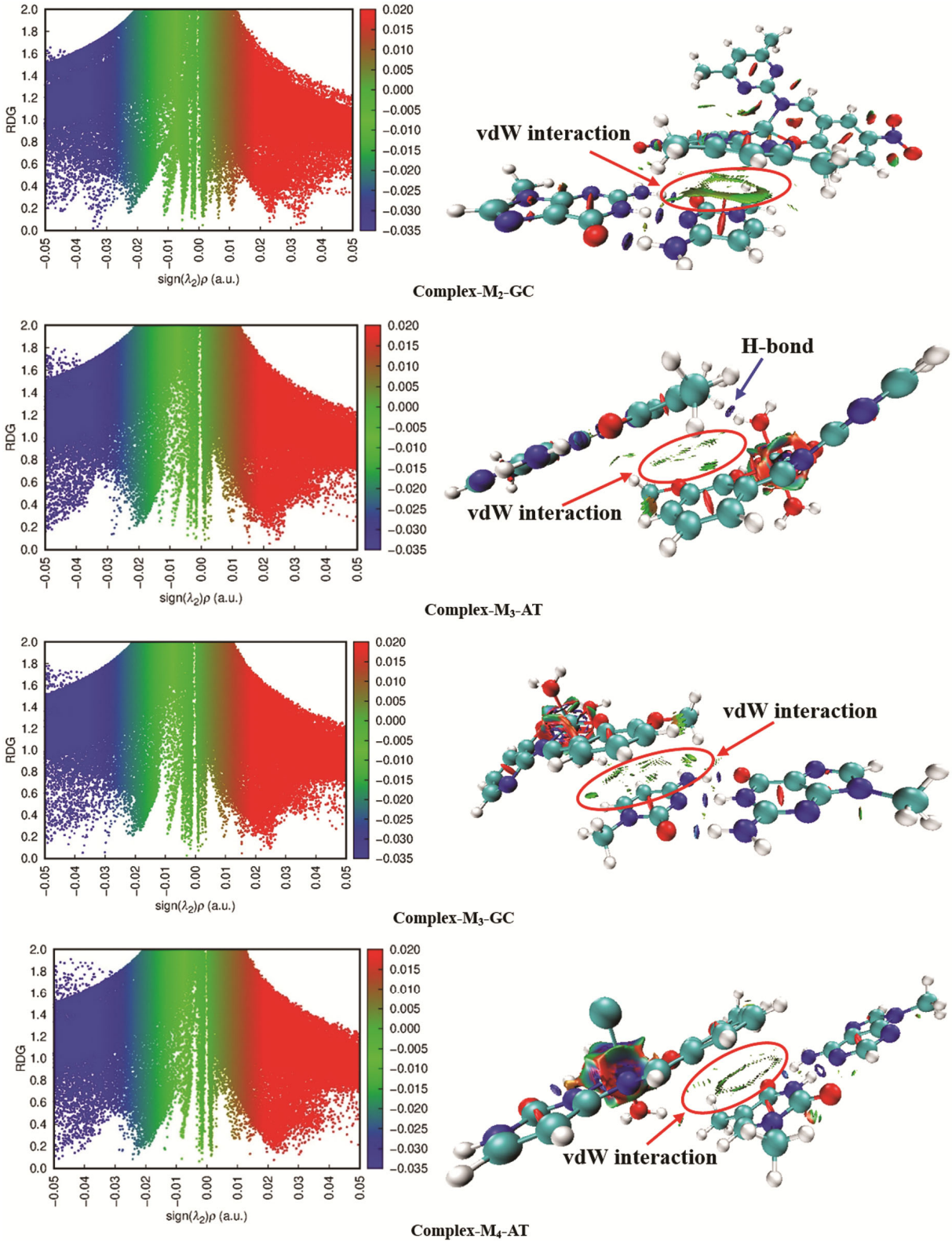

Fig. 5 — RDG scatter plots (left) and VMD plots (right) of stacked Co(II)-Schiff base-AT/GC base pair complexes (*Contd*.)

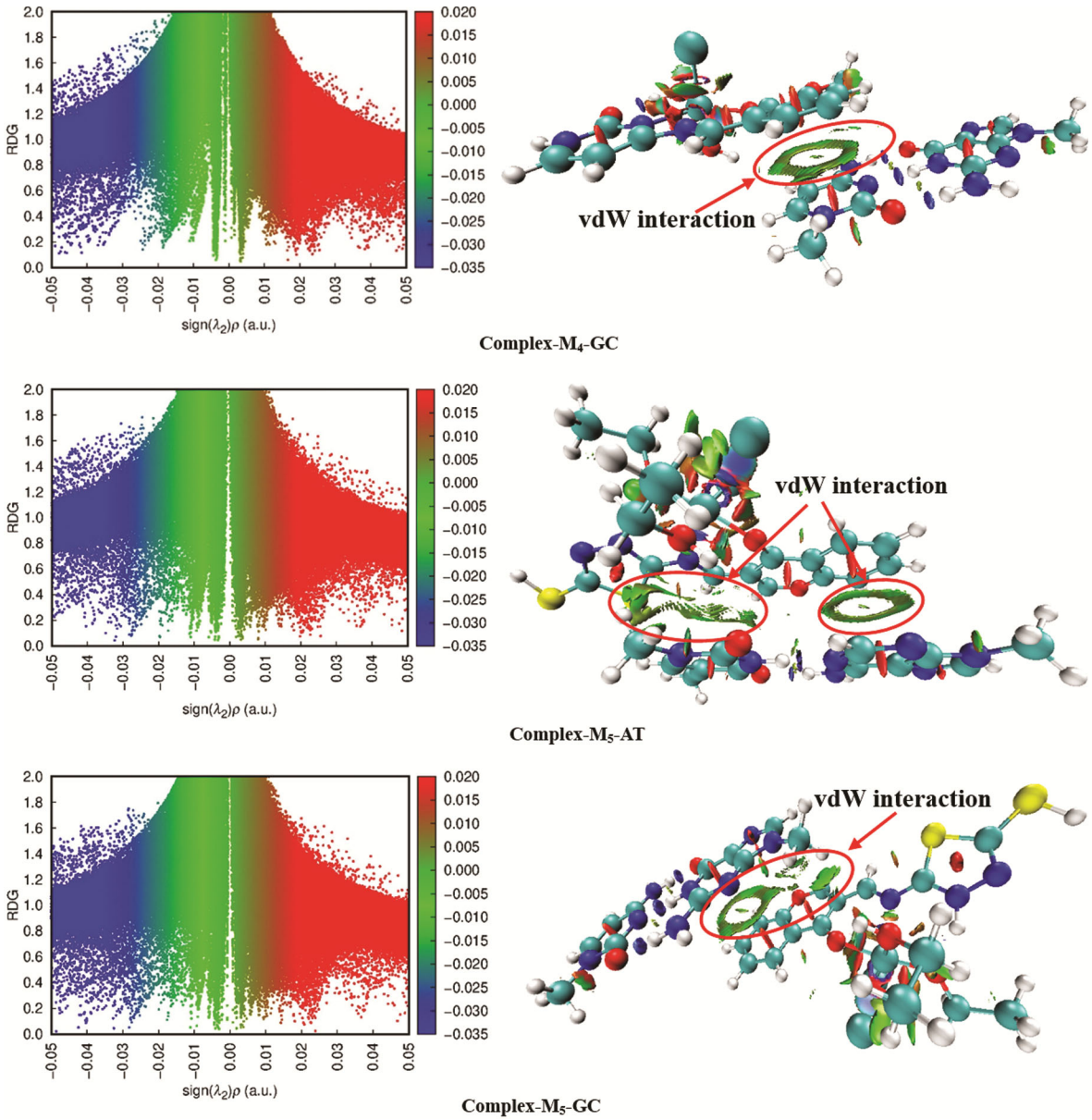

Fig. 5 — RDG scatter plots (left) and VMD plots (right) of stacked Co(II)-Schiff base-AT/GC base pair complexes

colour codes in real space; the blue-coloured isosurfaces on the left sides of the diagram depict the H-bonding interaction, whereas, the weak non-covalent molecular interactions are represented by the green colour. But, the red-coloured isosurface on the extreme right denotes the steric effect which results in strong repulsive forces exerted on the stacked complexes. The overall NCI plots of M_2, M_4 and M_5 complexes with GC-stacked systems were highly predominated over the AT-stacked systems. But interestingly, M_3-AT stacked complex shows stronger van der Waals interaction than that of the stacked GC complex. It is noteworthy that M_1 is the only anticancer agent, where both M_1-AT & M_1-GC stacked systems showed consistent van der Waals interaction. In addition, the VMD analysis shows the possible interacting region within a stacked molecular complex which are usually represented by green colour patches as shown in (Fig. 5). Therefore, RDG and VMD diagrams clearly illustrated the probable van der Waals interaction sites in all the stacked systems.

Molecular Docking analysis

Molecular docking and ligand activity analysis in drug-receptor molecular complexes are usually

influenced by electrostatic, hydrophobic and hydrogen bonding interaction[33,34]. For the mechanistic investigation of metal complexes and DNA nucleobases, the selected molecular complexes were prepared by using AutoDockTools v1.5.6 tool; further simulation and other calculations were done by AutoDock vina (The Scripps Research Institute, La Jolla, CA, USA)[35]. Herein, the molecular docking analysis of the selected Co(II)-Schiff base complexes with DNA duplex of sequence d(CGCGAATTCGCG)$_2$ dodecamer were carried out to preliminary forecast the binding sites and preferred orientation of sterically acceptable complex. The crystal structure of B-DNA dodecamer was obtained from the Protein Data Bank (PDB ID: 7RQT). Using AutoDock technologies, the heteroatoms around the duplex were first removed and then polar hydrogen atoms and Kollman united atom-type charges were added to the receptor molecule. The AD4 parameters for Co(II))-Schiff base complexes were set and all other settings were kept at default. The Grid box size and position were set in such a way that the entire dodecamer structure fell inside the grid box. After molecular docking, the complex was visualized in LigPlot+ and the optimal configuration was selected with the least amount of connection energy as a result.

Molecular docking study reveals that the complex, M_1 forms two H-bonds with the nitrogen at position-2 of the dGMP (10A) and dGMP (16B) with a bond length of 3.12 and 2.85Å, respectively (Fig. 6A-B). Another H-bond is formed with oxygen at position-2 of the dCMP (11A position) with a bond length of 3.21Å. Additionally, there also exists weak van der Waals interactions with surrounding dGMP (12A position), dAMP (18B position), dCMP (9A position) and dAMP (17B position) as shown in (Table 6). Similarly, M_2 forms one H-bond with Nitrogen at position-2 of the dGMP (4A position) with bond length of 3.26Å and other weak interactions with surrounding dCMP (21B position), dAMP (6A position), dTMP (7A position), dCMP (3A position), dAMP (5A position), dGMP (22B position) and dCMP (23B position). Complex M_3 forms two H-bonds with nitrogen at position-2 & 3, having bond lengths 3.04 and 2.98Å and forms another H-bond with Oxygen at position-4 of the dGMP (4A position). Moreover, it forms two additional H-bonds with Nitrogen at position-2 of the dGMP (22B position) with bond lengths 2.89 and 3.13Å. Complex M_4 forms one H-bond with Nitrogen at position-2 of the dGMP (22B position) and other weak interactions with dCMP (21B), dGMP (4A), dTMP (7A), dAMP (6A), dCMP (23B) and dAMP (5A); whereas, M_5 is the only anticancer agent among all the Co(II)-Schiff base agents which does not form any H-bond with DNA nucleobase; but shows other weak interactions with dAMP (6A position), dCMP (21B position), dGMP (4A position), dGMP (22B position), dCMP (23B position) and dGMP (24B position), respectively, as depicted in (Fig. 6A & B & Table 6).

It has been observed that -8.32 kcal/mol energy is released upon binding of M_1 to the binding pocket of B-DNA dodecamer. The optimum pose, having a binding energy of -8.32 kcal/mol was chosen out of the 9 poses generated for the M_1 complex. Similarly, -8.13 kcal/mol was chosen for M_2 complex, -8.21 kcal/mol for M_3 complex, -7.14 kcal/mol for M_4 complex, and -6.42 kcal/mol for M_5 complex as shown in (Table 6 & Fig. 6C). The LigPlot+ of the interaction, RasMOL diagram and docked position of Co(II)-Schiff base complexes in B-DNA dodecamer has been shown in (Fig. 6A-C).Based on the above analysis, M_1-B-DNA dodecamer appears to be the most stable complex with a binding energy of -8.32 kcal/mol. Hence, the sequence of stability of the Co(II)-based Schiff base complexes with respect to docking binding score is shown below:

$$M_5 < M_4 < M_2 < M_3 < M_1$$

ADMET screening

ADMET (absorption, distribution, metabolism, excretion, and toxicity) profiles of the chosen Co(II)-Schiff base complexes were evaluated using tools like SwissADME and STopTox[36]. This *in silico* analysis provided insights into their pharmacokinetics, drug-likeness, and potential toxicity, including specific risks like skin irritation, inhalation toxicity, and acute dermal toxicity[37,38]. This comprehensive assessment helps to identify potential safety concerns early in the drug development process. The bioavailability of a drug following oral administration greatly depends on its absorption within the intestine, which is a critical pharmacokinetic process[39]. Based on the results of the pharmacokinetics evaluation of the complexes presented in (Table 7A), most of the studied anticancer agents, excluding M_2 and M_5, displayed favourable intestinal absorption, suggesting good oral bioavailability. They exhibited diverse blood-brain barrier permeability, indicating potential interaction with P-glycoprotein and impacting their brain

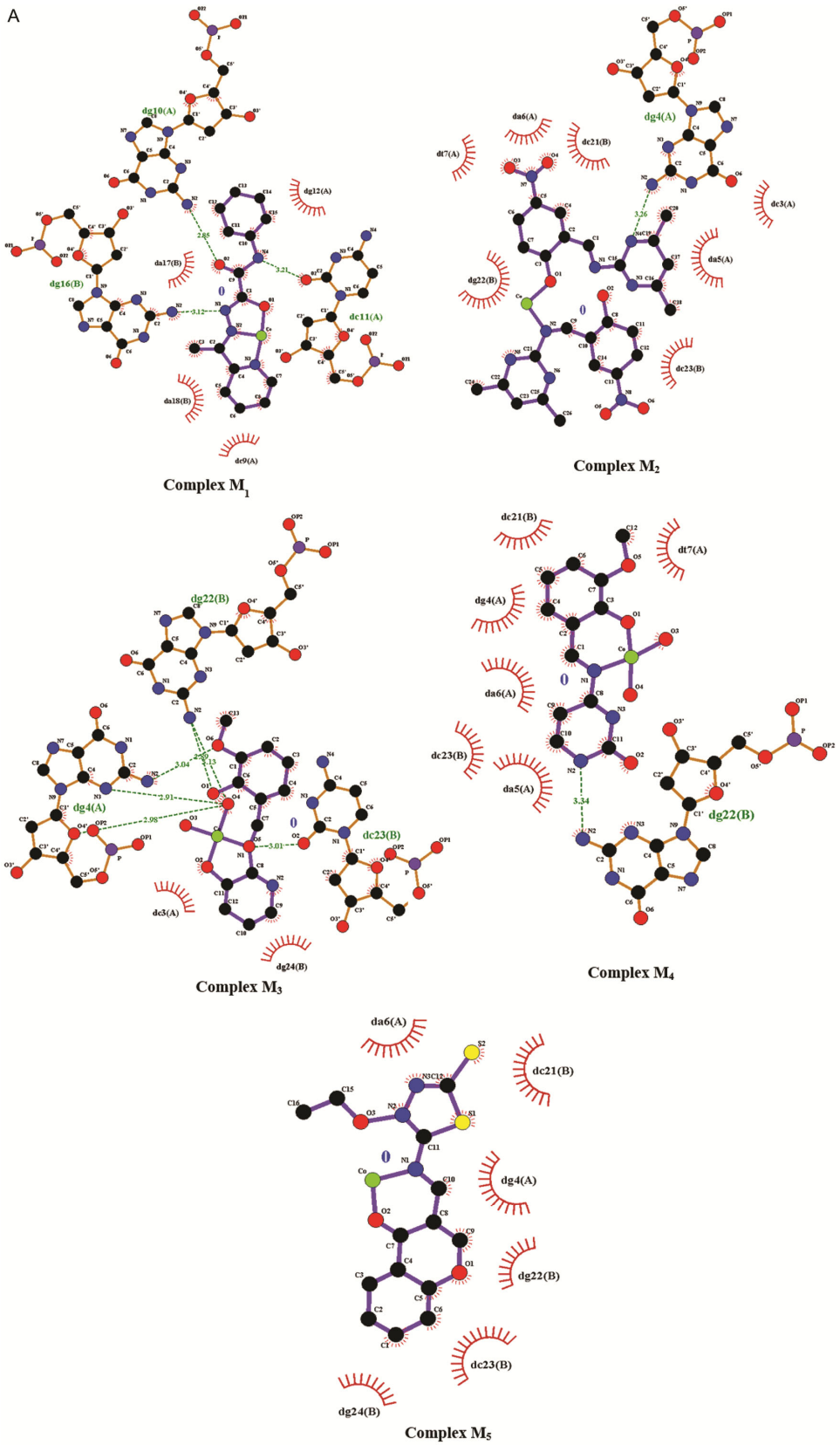

Fig. 6 — (A) The LigPlots of the interaction between Co(II)-Schiff base complexes and B-DNA dodecamer (*Contd.*)

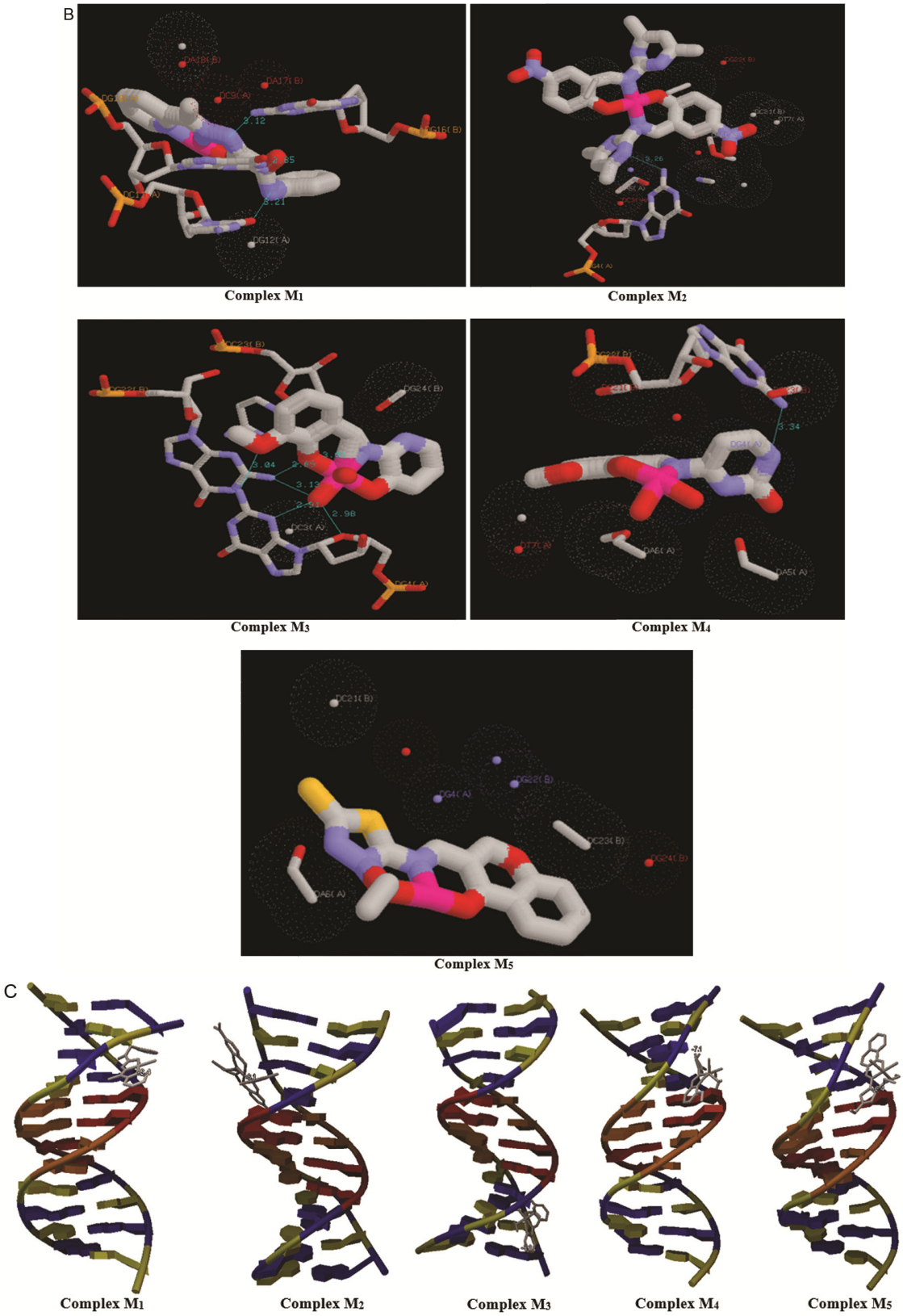

Fig. 6 — (B) RasMOL diagram showing the interaction of Co(II)-Schiff base complexes with B-DNA dodecamer; and (C) The docked position of Co(II)-Schiff base complexes in B-DNA dodecamer

Table 6− DNA docking data for Co(II) Schiff base complexes

Co(II) complexes	DNA residue	H-Bond distance (Å)	Other weak interactions	Total binding energy (kcal/mol)	Groove
M_1	dgMP16(B)	3.12	dgMP12(A)	-8.32	Minor
	dcMP11(A)	3.21	daMP18(B)		
	dgMP10(A)	2.85	dcMP9(A)		
			daMP17(B)		
M_2	dgMP4(A)	3.26	dtMP7(A)	-8.13	Minor
			daMP6(A)		
			dcMP21(B)		
			dcMP3(A)		
			daMP5(A)		
			dcMP23(B)		
			dgMP22(B)		
M_3	dgMP4(A)	2.91	dcMP3(A)	-8.21	Minor
		2.98	dgMP24(B)		
		3.04			
	dgMP22(B)	2.89			
		3.13			
	dcMP23(B)	3.01			
M_4	dgMP22(B)	3.34	dcMP21(B)	-7.14	Minor
			dgMP4(A)		
			dtMP7(A)		
			daMP6(A)		
			dcMP23(B)		
			daMP5(A)		
M_5	------	No H-bonding	daMP6(A)	-6.42	Minor
			dcMP21(B)		
			dgMP4(A)		
			dgMP22(B)		
			dcMP23(B)		
			dgMP24(B)		

Table 7A − Generated pharmacokinetic properties of the Co(II)-Schiff base complexes under study *via* SwissADME

	Pharmacokinetic Properties								
Complexes	GI (Gastro intestinal absorption)	Blood Brain Barrier (BBB) & Blood-Placenta Barrier (BPB)	Pgp-Substrate	CYP1A2 inhibitor	CYP2C19 inhibitor	CYP2C9 inhibitor	CYP2D6 inhibitor	CYP3A4 inhibitor	Log K_p (skin permeation) (cm/s)
M_1	High	No	Yes	No	Yes	No	No	No	-6.13
M_2	Low	No	Yes	No	Yes	Yes	No	Yes	-6.82
M_3	High	No	Yes	Yes	No	No	No	Yes	-7.94
M_4	High	No	Yes	Yes	No	No	No	No	-8.17
M_5	Low	No	Yes	Yes	Yes	No	Yes	Yes	-6.17

Table 7B − Generated druglikeness and medicinal properties of the complexes under study *via* SwissADME

	Druglikeness						Medicinal chemistry	
Complexes	LIPINSKI	GHOSE	VEBER	EGAN	MUGGE	Bioavailability Score	PAINS	Synthetic Accessibility
M_1	Yes; 0 violation	Yes; 0 violation	Yes; 0 violation	Yes; 0 violation	Yes; 0 violation	0.55	0 alert	4.43
M_2	No; 2 violations: MW>500, NorO>10	No; 2 violations: MW>480, MR>130	No; 1 violation: TPSA>140	No; 1 violation: TPSA>131.6	No; 2 violations: MW>600, TPSA>150	0.17	0 alert	5.49
M_3	Yes; 0 violation	Yes; 0 violation	Yes; 0 violation	Yes; 0 violation	Yes; 0 violation	0.55	0 alert	3.89
M_4	Yes; 0 violation	Yes; 0 violation	Yes; 0 violation	Yes; 0 violation	Yes; 0 violation	0.55	0 alert	4.08
M_5	Yes; 1 violation: MW>500	No; 1 violation: MW>480	No; 1 violation: TPSA>140	No; 1 violation: TPSA>131.6	No; 1 violation: TPSA>150	0.11	0 alert	4.30

(*Contd*.)

Table 7C− Generated Toxicity profiles of the complexes under study *via* STopTox (*Contd*.)

	Toxicity parameters using STopTox			
Complexes	Acute Inhalation Toxicity	Acute Dermal Toxicity	Skin Sensitization	Skin Irritation and Corrosion
M_1	Non-Toxic (-)	Non-Toxic (-)	Non-Sensitizer (-)	Negative (-)
M_2	Non-Toxic (-)	Non-Toxic (-)	Sensitizer (+)	Negative (-)
M_3	Non-Toxic (-)	Non-Toxic (-)	Non-Sensitizer (-)	Negative (-)
M_4	Non-Toxic (-)	Non-Toxic (-)	Non-Sensitizer (-)	Negative (-)
M_5	Non-Toxic (-)	Non-Toxic (-)	Non-Sensitizer (-)	Negative (-)

accessibility. In terms of metabolism, complexes M_1 and M_2 act as substrates for CYP1A2, while M_3 and M_4 target CYP2C19. M_1, M_3, and M_4 act on both CYP2C9 and CYP2D6, potentially affecting drug interactions. Additionally, M_1 and M_4 target CYP3A4, while other complexes inhibit their respective isoforms as shown in (Table 7A). All complexes demonstrated moderate skin permeability, highlighting their limited penetration potential. This combined analysis provides valuable insights into their pharmacokinetic behaviour and potential drug interactions. Moreover, *in silico* analyses revealed moderate skin permeation of the studied anticancer agents, as evidenced by Log K_p values ranging from -6.13 to -8.17 cm/s. Notably, a more negative Log K_p signifies diminished skin permeability.

Again, the physicochemical properties play a crucial role in drug-likeness assessment methodologies, which include the "Rule of Five" (Ro5), Veber rules, Egan's criteria, and the Ghose filter[40-42]. Most Co(II) complexes, except M_2 and M_5, passed key drug-likeness filters like "Rule of Five" and Veber rules, suggesting good oral bioavailability. Again, the Bioavailability Score predicts a compound's likelihood of having bioavailability over 10% in rats or measurable Caco-2 permeability. Passing Lipinski's rule-of-five grants a favourable pharmacokinetic Bioavailability Score of 0.55, while failing assigns a score of 0.11[43]. Most of the Co(II) complexes had a bioavailability Score of 0.55, signifying good pharmacokinetic potential; while complexes M_2 and M_5 scored lower (0.11 and 0.17), implying limited oral absorption potential (Table 7B). Fortunately, all studied Co(II) complexes passed the PAINS (Pan Assay Interference compounds) analysis, indicating the absence of problematic structures that interfere with various assays regardless of the target[44]. Additionally, their Synthetic Accessibility (SA) Scores (3.89 - 5.49) fell within the ideal range (1-10), suggesting feasible synthesis (Table 7B). However, the toxicity profile showed no concerns for most of the complexes, except M_2, which exhibited indications of skin sensitization as depicted in (Table 7C).

Conclusion

Among the studied Co(II)-Schiff base complexes, Complex M_1 demonstrates a strong preference for binding to both AT and GC base pairs, evident from its significantly negative interaction energy of -18.55 and -23.42 kcal/mol, respectively. Conversely, Complex M_5 exhibits the weakest interaction with the least negative interaction energies. Significantly, all complexes exhibited a preference for GC base pairs, suggesting targeted interaction potential. HOMO-LUMO analysis provided valuable physicochemical information like chemical potential, hardness, softness, and electrophilicity. Additionally, MEP diagrams revealed the active sites of these complexes. NBO analysis uncovered differences in electronic transitions between unstacked and stacked models, offering deeper insights into their behaviour. Furthermore, NCI and VMD analyses confirmed predicted electron density shifts, interaction sites, and binding modes for the preferred stacked models, validating prior computational studies. Molecular docking studies confirmed H-bonding and other weak interactions with B-DNA dodecamer, with M_1 exhibiting the most stable binding and highest docking score. In addition, ADMET screening ensured both safety and efficacy by evaluating the pharmacokinetics, bioavailability, toxicity, metabolism, and potential interactions.

Conflict of interest

All authors declare no conflict of interest.

References

1 Kiraz AÖ, Theoretical insight into the antioxidant, electronic and anticancer behaviour of *simmondsin*. *Indian J Biochem Biophys*, 57 (2020) 530.

2 Genevieve H, Shannon B, Sarah H, Karolina L, Mckenna L, Nicole S & Sibaji S, Drug resistance in cancer: an overview. *Cancers*, 6 (2014) 1769.

3 Saranya, J, Jone KS, Chitra S, Zarrouk A, Kalpana K, Lavanya K & Ravikiran B, Tetradentate Schiff Base complexes of transition metals for antimicrobial activity. *Arab J Sci Eng*, 45 (2020) 4683.

4 Shweta S, Synthesis, spectroscopic studies and pesticidal activity of transition metal complexes with unsymmetrical schiff base. *Indian J Biochem Biophys*, 58 (2021) 565.

5 Nooshin K, Alison Z & Sheida E, Bioactive Ni (II), Cu (II) and Zn (II) complexes with an N3 functionalized Schiff base ligand: Synthesis, structural elucidation, thermodynamic and DFT calculation studies. *Inorganica Chim Acta*, 54 (2022) 121083.

6 Panchangam MK, Katreddi HR, Jay Prakash P & Dayananda S, Synthesis, characterization, DNA binding and nuclease activity of binuclear copper (II) complexes of cuminaldehyde thiosemicarbazones. *Transit Met Chem*, 33 (2008) 661.

7 Ömer Ş, Ümmühan Ö, Nurgül S, Zuhal Karagöz G, Kerem K, Burcu A, Suat T & Zeynel S, New platinum (II) and palladium (II) complexes of coumarin-thiazole Schiff base with a fluorescent chemosensor properties: Synthesis, spectroscopic characterization, X-ray structure determination, *in vitro* anticancer activity on various human carcinoma cell lines and computational studies. *J Photochem Photobiol B Biol*, 178 (2018) 428.

8 Virendra RM, Chaitannya WG, Suraj NM, Hemchandra KC & Nagaiyan S, Schiff base clubbed benzothiazole: synthesis, potent antimicrobial and MCF-7 anticancer activity, DNA cleavage and computational study. *J Biomol Struct Dyn*, 38 (2019) 1772.

9 Zenat MZ, Sawsan SH & Amina AS, Studies on some Schiff base complexes of CoII, NiII and CuII derived from salicylaldehyde and o-nitrobenzaldehyde. *Spectrosc Lett*, 31 (1998) 757.

10 Moghadam NH, Salehzadeh S, Shahabadi N, Spectroscopic and molecular docking studies on the interaction of antiviral drug nevirapine with calf thymus DNA. *Nucleosides Nucleotides Nucleic Acids*, 36 (2017) 553.

11 Sachin AD, Umesh B, Umakant BC, DJ S, Ubale PA, Shashikant HG & Shiva Prasad K, Newly synthesized triazole-based Schiff base ligands and their Co (II) complexes as antimicrobial and anticancer agents: Chemical synthesis, structure and biological investigations. *Results Chem*, 3 (2021) 100162.

12 Kanisha K, Diya G, Bikash K & Arpita C, A concise review on cobalt Schiff base complexes as anticancer agents. *Polyhedron*, 222 (2022) 115890.

13 Ola A EG, GM Abu ER, Tarek AY, Mohamed M, Synthesis, spectral characterization, computational calculations and biological activity of complexes designed from NNO donor Schiff-base ligand. *Spectrochim Acta A Mol Biomol Spectrosc*, 146 (2015) 163.

14 Nagaraj R, Murugesan S, Jegathalaprathaban R & Jeyaraj DR, Biologically active Cu (II), Co (II), Ni (II) and Zn (II) complexes of pyrimidine derivative Schiff base: DNA binding, antioxidant, antibacterial and *in vitro* anticancer studies. *J Fluoresc*, 27 (2017) 1801.

15 Laila H AR, Abu-Dief AM, Rafat M EK, Shimaa M AF, Sonochemical synthesis, DNA binding, antimicrobial evaluation and *in vitro* anticancer activity of three new nano-sized Cu (II), Co (II) and Ni (II) chelates based on tri-dentate NOO imine ligands as precursors for metal oxides. *J Photochem Photobiol B Biol*, 162 (2016) 298.

16 Mehmet EA, Ünzile K, Yusuf A, Nevin T & Kenan B, Cobalt and ruthenium complexes with pyrimidine based schiff base: Synthesis, characterization, anticancer activities and electrochemotherapy efficiency. *J Mol Struct*, 1226 (2021) 129402.

17 Mohamed G, Nadia EW, Kamal EB & Sara H, Chromone Schiff base complexes: synthesis, structural elucidation, molecular modeling, antitumor, antimicrobial, and DNA studies of Co (II), Ni (II), and Cu (II) complexes. *J Iran Chem Soc*, 16 (2019) 169.

18 Manisha Y & Eswari JS, Evolution of modern age drug discovery of lipopeptides and computer-aided drug discovery in India. *Indian J Biochem Biophys*, 59 (2022) 503.

19 Trilaksana H, Thanmayalaxmi D & Suvitha A, ADMET, Pharmacokinetic and Docking properties of the fungal drug 2-(2, 4-difluorophenyl)-1, 3-bis (1, 2, 4-triazol-1-yl) propan-2-ol by using Quantum computational methods. *Indian J Biochem Biophys*, 60 (2022) 58.

20 Anurag A, Giriraj K & Lakshmayya T, Molecular docking study to elucidate the anti-pruritic mechanism of selected natural ligands by desensitizing TRPV3 ion channel in Psoriasis: An *in silico* approach. *Indian J Biochem Biophys*, 57 (2020) 578.

21 Roy D, Todd K & John M, GaussView, version 5 (2009).

22 Frisch, MJ, TrucksGW, Schlegel HB, Scuseria GE, Robb MA, Cheeseman JR, Scalmani G, Barone V, Mennucci B, Petersson GA & Nakatsuji H, Gaussian 09, (2009).

23 Pratyashee B, Benzir A & Bipul B, Some Pt (II)-complexes with dpb, Fdpb and F2dpb ligands as potent anticancer agents and their mode of interaction with AT/GC base pairs: A DFT study. *J Indian Chem Soc*, 100 (2023) 100923.

24 Abduvakhid J, Holikulov U, Hushvaktov H, Issaoui N & Absanov A, Intermolecular interactions in ethanol solution of OABA: Raman, FTIR, DFT, M062X, MEP, NBO, FMO, AIM, NCI, RDG analysis. *J Mol Liq*, 377 (2023) 121552.

25 Jun-ichi A, Reduced HOMO− LUMO gap as an index of kinetic stability for polycyclic aromatic hydrocarbons. *J Phys Chem A*, 103 (1999) 7487.

26 Senet P, Chemical hardnesses of atoms and molecules from frontier orbitals. *Chem Phys Lett*, 275 (1997) 527532.

27 Alan ER, Larry AC & Frank W, Intermolecular interactions from a natural bond orbital, donor-acceptor viewpoint. *Chem Rev*, 88 (1988) 899.

28 Sowrirajan S, Elangovan N, Ajithkumar G & Manoj KP, (E)-4-((4-Bromobenzylidene) amino)-N-(Pyrimidin-2-yl) benzenesulfonamide from 4-bromobenzaldehyde and sulfadiazine, synthesis, spectral (FTIR, UV–vis), computational (DFT, HOMO–LUMO, MEP, NBO, NPA, ELF, LOL, RDG) and molecular docking studies. *Polycycl Aromat Compd*, 42 (2022) 7616.

29 Julia CG, Ionic interactions: Comparative topological approach. *Comput Theor Chem*, 998 (2012) 193.

30 Tian L & Chen F, Multiwfn: A multifunctional wave function analyzer. *J comput chem*, 33 (2012) 580.

31 Humphrey W, Andrew D & Klaus S, VMD: Visual molecular dynamics. *J mol graph*, 14 (1996) 33.

32 Nipu KD, Dhirendra KM, Papu KN, Pyarimohan D, Suryasarathi B & Tamal B, Dihydrolevoglycosenone as a novel bio-based nanofluid for thermal energy storage: Physiochemical and quantum chemical insights. *J Energy Storage*, 59 (2023) 106365.

33 Davut A, Sümeyye A, Fatih S, Ömer T, Adil B, Yusuf A, Belma ZK & Necmi D, Novel metal complexes containing 6-methylpyridine-2-carboxylic acid as potent α-glucosidase inhibitor: synthesis, crystal structures, DFT calculations, and molecular docking. *Mol Divers*, 25 (2021) 171.

34 Aditya LT, Manisha Y, Swasti D, Seenivasan A & Jujjavarapu SE, Molecular docking and ADMET analysis of synthetic statins for HMG-CoA reductase inhibition activity. *Indian J Biochem Biophys*, 58 (2021) 127.
35 Oleg T & Arthur JO, AutoDock Vina: improving the speed and accuracy of docking with a new scoring function, efficient optimization, and multithreading. *J Comput Chem*, 31 (2010) 455.
36 Antoine D & Olivier M, SwissADME: a free web tool to evaluate pharmacokinetics, drug-likeness and medicinal chemistry friendliness of small molecules. *Sci Rep*, 7 (2017) 42717.
37 John CD, Toxicology, *In silico* prediction of ADMET properties: how far have we come? *Expert Opin Drug Metab Toxicol*, 3 (2007) 635.
38 Saumya S & Anjana P, Computational screening of anticancer drugs targeting miRNA155 synthesis in breast cancer. *Indian J Biochem Biophys*, 57 (2020) 389.
39 Andrew F & Peter P, P-glycoprotein and its role in drug-drug interactions. *Aust Prescr*, 37 (2014) 137.
40 Daniel FV, Stephen RJ, Hung-Yuan C, Brian RS, Keith WW & Kenneth DK, Molecular properties that influence the oral bioavailability of drug candidates. *J Med Chem*, 45 (2002) 2615.
41 William JE, Kenneth MM & John JB, Prediction of drug absorption using multivariate statistics. *J Med Chem*, 43 (2000) 3867.
42 Arup KG, Vellarkad NV & John J, A knowledge-based approach in designing combinatorial or medicinal chemistry libraries for drug discovery. 1. A qualitative and quantitative characterization of known drug databases. *J Comb Chem*, 1 (1999) 55.
43 Christopher AL, Franco L, Beryl WD & Paul JF, Experimental and computational approaches to estimate solubility and permeability in drug discovery and development settings. *Adv Drug Deliv Rev*, 23 (1997) 3.
44 Jonathan BB & Georgina AH, New substructure filters for removal of pan assay interference compounds (PAINS) from screening libraries and for their exclusion in bioassays. *J Med Chem*, 53 (2010) 2719.